n³l - Int'l Summer School and Workshop on Non-Normal and Nonlinear
Effects in Aero- and Thermoacoustics, June 18 − 21, 2013, Munich

n^3l

CHARACTERISTICS OF DYNAMIC PRESSURE DATA AND FLAME STRUCTURES IN AN UNSTABLE LEAN PREMIXED COMBUSTOR WITH MIXTURE INHOMOGENEITY

Shigeru Tachibana*[1], Atsushi Fukumoto[2], Kota Kanai[2], Seiji Yoshida[1],
Kazuo Suzuki[1], Tetsuya Sato[3], Hiroshi Gotoda[4]

[1] Institute of Aeronautical Technology, Japan Aerospace Exploration Agency
7-44-1 Jindaiji-Higashii, Chofu, Tokyo 182-8522, Japan
[2] Graduate School of Fundamental Science and Engineering, Waseda University
3-4-1, Okubo, Shinjuku, Tokyo169-8555, Japan
[3] School of Fundamental Science and Engineering, Waseda University
3-4-1, Okubo, Shinjuku, Tokyo169-8555, Japan
[4] Department of Mechanical Engineering, Ritsumeikan University
1-1-1 Nojihigashi, Kusatsu-shi, Shiga 525-8577, Japan
* Corresponding author: tachibana.shigeru@jaxa.jp

As a nonlinear time series analysis, the translation error method is applied to the dynamic pressure data of a lean premixed model combustor. It is shown that the method successfully captures the transitions of the combustor stability and there is a deterministic nature in the parallelism of neighboring trajectories of the data under strong pressure oscillations. Then, dynamic behaviors of inhomogeneous mixture flames are investigated from the phenomenological aspect by applying optical diagnostics. In the strong oscillations case, a bulge of fresh gas, which is considered a traveling vortex ring of fresh gas mixture, is periodically moving along the outer shear layer and merging with the stationary vortex flame near the wall. The level of the vortex-flame interaction is very sensitive to the local equivalence ratio distribution, and it seems that the strong oscillations occur when richer mixtures locate about the inner shear layer region. These observations indicate that the driving force of the instability is the vortex-flame interaction, but the strength of the instability is modified by the local distribution of equivalence ratio.

1 Introduction

Combustion instability has become a main technical challenge in the development of low-emission combustors of aero and industrial gas-turbine engines as it may cause catastrophic damages to combustion chambers and, in some cases, other engine components. There has been a great deal of studies on this issue in the past decades [1], but the problem is not fully resolved yet due to the complexity of the phenomenon. For instance, in a jet-engine lean-premixed combustor, dynamic flame response characteristics are determined by the processes of atomization, vaporization, fuel-air mixing, vortices-flame interactions, acoustic wave propagation, and so on. These processes are simultaneously going on under high temperature and high pressure environment. Understanding the processes is definitely a key technology for realizing stable combustion along with the instability suppression control technologies.

In this work, characteristics of the dynamic pressure data and unsteady flame structures observed

in a lean premixed gas-turbine model combustor under self-excited combustion instabilities are investigated. The low-swirl injector (LSI), which is known for ultra-low emissions performance, is implemented for flame holding. The LSI was originally developed at the Lawrence Berkeley National Laboratory for turbulent premixed flame studies [2]. Recently, many studies have been devoted to the adaptation of the technology to fuel-flexible gas turbines. (e.g., [3–5]). Dynamic features of low-swirl flames have been investigated by several groups [6–10]. Tachibana et al. [6] stdudied dynamic responses of the turbulent flame brush and flame surface density in the core flow region under global stretch rate oscillations. It was found that there was a direct relationship between the global heat-release and flame surface area oscillations. Kang et al. [7] investigated the dynamic structures of the flame under acoustic forcing and found a series of toroidal structures in the shear layer mixing zone. The wave number of the toroidal structures and the excitation frequency were correlated at lower frequencies (<65Hz). Huang and Ratner [8] studied the interaction between acoustic excitation and the shear layer vortices and clarified that the changes in heat release were driven by changes in the amount of flame surface. More recently, Therkelsen et al. [9] reported unstable flame behaviors of CH_4 and H_2/CH_4 flames under self-excited combustion instabilities. Phase-resolved PIV measurements of CH_4 flame showed that ring vortices were shed from the LSI rim and that their convection speed along the outer shear layer (OSL) corresponded to the dominant frequency of the acoustic and flame oscillation spectra. The trailing edge of the flame brush impinged on the combustor wall and the vortices were trapped below this impingement point. Davis et al. [10] characterized the flame/vortex interaction processes of the two unstable flames. The Rayleigh index showed more regular and stronger driving in the H_2/CH_4 flame than in the CH_4 flame. This was due to the merging of the central flat region of the H_2/CH_4 flame with the rolled-up structures in the OSL resulting in a narrow region with high heat release density. All these experiments have been targeting homogeneous mixture flame dynamics, while the goal of this study is to clarify the effect of mixture inhomogeneity on the flame dynamics. In practical gas-turbines, fuel is injected at a certain distance upstream from the combustor inlet, and shorter mixing distances are requested for avoiding flame flashback and/or auto-ignition events. Hence, it is more practical that there are inhomogeneous fuel distributions in the incoming flows to the combustion chambers, and it is crucial to understand the effects of mixture inhomogeneity on combustor stability.

Nonlinear time series analysis based on dynamical system theory has been applied to experimental data in a wide spectrum of research fields [11]. The analysis has been applied to characterize the nonlinear features of combustion instabilities and flame front dynamics from the viewpoint of the self-similar structure and orbital instability in a phase space by utilizing the correlation dimension, multifractal and Lyapunov exponent (e.g., [12–17]) There is another simple and useful nonlinear time series analysis based on orbital instability in phase space for distinguishing chaos from a stochastic process, referred to as the translation error method [18]. The translation error represents the degree of parallelism of trajectories in the phase space, which has been used to successfully characterize the dynamic properties of different types of flame front instability [14]. Recently, Gotoda et al. [19, 20] investigated nonlinear characteristics of dynamic pressure data of a preheated lean-premixed gas-turbine model combustor and showed that, with decreasing equivalence ratio, a significant transition from periodic oscillation generated by thermoacoustic combustion oscillations to fractional Brownian motion in close proximity to LBO through chaos. [17]

In this paper, the translation error analysis is applied to the dynamic pressure data of the combustor with both homogeneous and inhomogeneous mixture cases so as to characterize the nonlinearity in the data. Then, from the phenomenological aspect, dynamic behaviors of the inhomogeneous mixture flames are investigated by the OH* chemiluminescence and laser Mie scattering image analyses.

2 Experimental Configurations

2.1 Experimental Setup and Conditions

Figure 1 shows the schematic of the experimental setup. The low-swirl injector which was developed jointly with Lund University and Technische Universität Darmstadt [21] is used in this study. The LSI nozzle has an inner diameter of 50 mm, with a swirler (downstream end) placed 68mm upstream of its

exit plane. The annular section of the swirler is fitted with eight constant thickness curved vanes, each having a discharge angle of 37 deg. The central channel is 38mm in diameter, and is fitted with a perforated plate that has 37 holes of 3mm diameter. The holes are arranged in a hexagonal/radial pattern. It was reported in the literature [21] that the effective swirl number of this nozzle was approximately 0.55. The combustion chamber is composed of an inlet face plate and a cylindrical quartz glass tube whose length and inner diameter were 495 and 146 mm, respectively. Methane gas is used as fuel. There are two fuel supply lines. Primary fuel is injected upstream of a static mixer before entering the burner setup. Secondary fuel is injected into the burner through 12 orifices of 1 mm diameter at the axial location 143.5 mm upstream of the combustion chamber inlet. Fuel mixedness can be parametrically modified by changing the fuel split, while keeping the total fuel flow rate (i.e. total equivalence ratio) constant. The experiments were carried out under atmospheric pressure and ambient temperature.
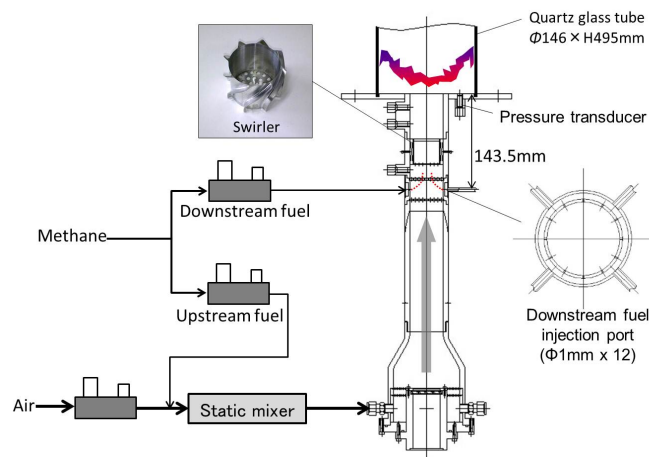

Figure 1: Schematic of the experimental setup.

2.2 Measurement Setup

A pressure transducer (Kulite WCT-312-5SG) is flush-mounted on the face plate of the combustion chamber to measure dynamic pressure. A high-speed camera (Photron FASTCAM-APX) is used for OH* chemiluminescence imaging at a sampling rate of 5,000 Hz. The spatial resolution is 640*640 pixels (0.26mm/pixel). An image intensifier (Lambert HiCATT 25D) is connected to the camera with a relay optics. Gate width of the I.I. is 60 μ sec. A UV lens (Sodern Cerco2178 F/2.8, 100mm) and an optical band-pass-filter (Semrock FF01-320/40) are mounted. Start trigger and gate timing of the image intensifier and dynamic pressure signals are simultaneously recorded on a multi-channel data recorder at a 102.4 kHz sampling rate. Phase-locked average process is applied to the pressure signals and OH* images based on the time-series signals. Meanwhile, the sampling rate of the dynamic pressure data used for the spectral and E_{trans} calculation is 5.12kHz.

The laser Mie scattering measurement is performed with the oil mist seeding. The 6-jet atomizer (TSI) with the DEHS (Di-Ethyl-Hexyl-Sebacate) oil is used for generating the oil mist. The Nd:YAG laser Gemini-PIV of New Wave Research is used with the 80 mJ pulse power at 532nm. The CCD camera is the Imager Pro X 4M (LaVision, 2048x2048 pixels). A camera lens (Nikon AF MICRO NIKKOR 105mm 1:2.8D) and an optical band-pass-filter (CVI Laser Optics F03-532.0-4-2.00) are mounted on the CCD. The spatial resolution is 0.07mm/pixel. The timing of laser emission is monitored and recorded simultaneously with the dynamic pressure data at a sampling rate of 102.4 kHz so that the phase-locked analysis can be applied in the same way as the chemiluminescence measurement.

3 Data Analysis

3.1 Time Series Data Analysis

3.1.1 Translation Error

If the determinism is clearly visible in a time series data obtained in experiments, the neighboring trajectories in the phase space will have similar directions. However, as the determinism is lost, the trajectories diverge with time owing to the orbital instability in the phase space. On the basis of this concept, we introduce a useful algorithm proposed by Wayland et al. [18] to extract the determinism from complex time series data obtained in experiments. A phase space based on Takens' embedding theorem [22] is first constructed from the time-series data of p'. The time-delayed coordinates used for the construction of the phase space are expressed as

$$\boldsymbol{p}'(t_i) \quad = \quad \left(p'(t_i)\,,\; p'(t_i+\tau)\,,\; p'(t_i+2\tau)\,,\; \cdots,\; p'(t_i+(D+1)\tau) \right) \tag{1}$$

where $i = 0, 1, \cdots, n$ (n is the number of data of the time series), $\boldsymbol{p}'(t_i)$ are the phase space vectors, $p'(t_i)$ are the dynamic pressure data at time t_i, D is the embedding dimension (the dimension of the phase space) and τ is the time lag. In this work, D is set to 3. τ is determined for each data by the mutual information calculation as reported in the previous study [19]. It turned out that $\tau = 4$ was appropriate for all the data in this paper.

After randomly selecting a vector $p'(t_i)$ from the phase space, we find its K nearest neighbors $p'(t_k)$ with k from 1 to K. In this work, K is set to 100. By setting the images of all the vectors to $p'(t_k + T)$ at a suitable time interval T, the diversity in the directions of neighboring trajectories is measured in terms of the translation error E_{trans}, defined by

$$E_{\text{trans}} \quad = \quad \frac{1}{K+1} \sum_{k=0}^{K} \frac{\| \boldsymbol{v}(t_k) - \overline{\boldsymbol{v}} \|^2}{\| \overline{\boldsymbol{v}} \|^2}\,, \tag{2}$$

$$\overline{\boldsymbol{v}} \quad = \quad \frac{1}{K+1} \sum_{k=0}^{K} \boldsymbol{v}(t_k)\,. \tag{3}$$

In this work, T is set to 8. Here, $\boldsymbol{v}(t_k)(= p'(t_k + T) - p'(t_k))$ approximates the tangential vectors of trajectories at time t_k. The more parallel the trajectories are to each other, that is, the more visible determinism there is in the time series, the closer E_{trans} will be to zero. In the estimation of the translation error, the stochastic error can be reduced by obtaining the medians of E_{trans} for Q sets of M randomly chosen $p'(t_i)$ and then taking the mean of the Q medians. In this work, M and Q are set to 100 and 10, respectively.

3.1.2 Damping Factor (Bandwidth Method)

Figure 2 shows the definition of the damping factor with bandwidth method. The damping factor is normally used for evaluating the effectiveness of damping devices (e.g., [23]), but it can also be used for health monitoring purposes. Lieuwen [24] proposed a method to monitor combustor's stability margin using dynamic pressure data. In his case, the damping coefficient which has a direct relation to the decay rate of the envelope of the autocorrelation of the dynamic pressure data was utilized. In this paper, the bandwidth method is applied to the dynamic pressure data and compared to the E_{trans}.

3.2 Laser Sheet Mie Scattering Image Analysis

The Mie scattering images of the oil mist is post-processed to estimate the so-called $\bar{c}_{\text{Mie}}$ distribution. The binarization procedure is shown in Figure 3 from (a) to (d). The edge of the dense region can be considered as an iso-thermal boundary at the boiling point of DEHS (~529 K). A Gaussian filter (5 by 5 pixels) and the anisotropic diffusion filter of Peroma and Malik [25] (with parameters $N_{iter} = 10$, $\Delta t =$

S. Tachibana, A. Fukumoto, K. Kanai, S. Yoshida, K. Suzuki, T. Sato, H. Gotoda
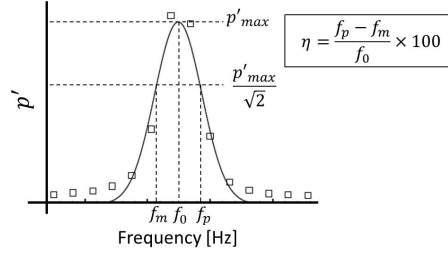

$$\eta = \frac{f_p - f_m}{f_0} \times 100$$

Figure 2: Definition of the damping factor with bandwidth method (η). The dominant peak (the first peak) is detected in the power spectrum, then the Gaussian fitting is applied on the five adjacent points around the peak.
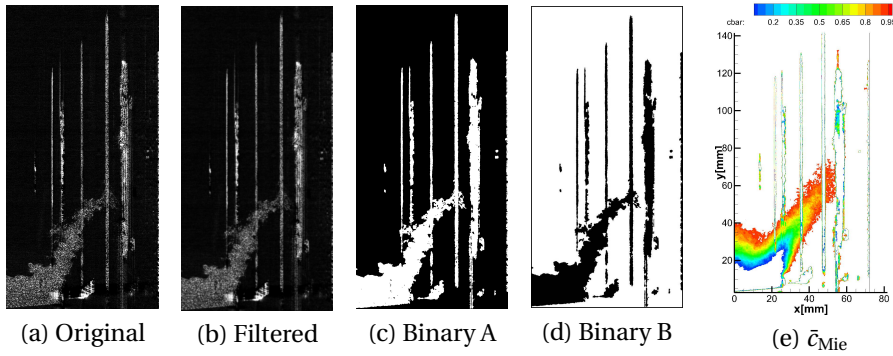

(a) Original (b) Filtered (c) Binary A (d) Binary B (e) $\bar{c}_{\text{Mie}}$

Figure 3: Image processing of the laser Mie scattering images for calculating $\bar{c}_{\text{Mie}}$. Only the right hand side half plane is shown. The $\bar{c}_{\text{Mie}}$ contour between 0.05-0.95 is shown in (e).

$1/7$, $\kappa = 100$, $C_{cond} = 1/(1+(\nabla I/\kappa)^2)$) are applied to the original image (Figure 3(b)). The filtered image is binarized by a simple threshold method (Figure 3(c)) and then flipped (Figure 3(d)). In Figure 3(d), black (I=0) means the fresh gas region and white (I=1) means the high temperature region beyond the boiling point. Note that the vertical streaky patterns appeared in the images are due to laser sheet reflections on the glass tube surfaces. Finally, the $\bar{c}_{\text{Mie}}$ distribution is derived by averaging multiple binary B images as shown in Figure 3(e).

4 Results and Discussion

4.1 Spectral and nonlinear time-series analyses of the dynamic pressure data

4.1.1 Homogeneous mixture flame results

Figure 4 shows the transition of the pressure power spectrum when increasing equivalence ratio from 0.60 to 0.85 with a constant bulk air flow velocity of 12.5 m/s. Strong pressure oscillations whose peak amplitudes exceed 1 kPa are observed for $\phi = 0.66 - 0.71$. The largest amplitude in this data is $p'_{\text{p-p}} = 3.55$ kPa at $\phi = 0.68$. The peak frequency slightly increased from 323 Hz at $\phi = 0.66$ to 343 Hz at $\phi = 0.71$. Below $\phi = 0.66$, low-amplitude single peaks are seen about 310Hz. On the other hand, for $0.72 \le \phi \le 0.85$, there are low-amplitude double peaks. To look at the trends more in detail, peak frequencies are plotted against equivalence ratios in Figure 5. When looking at the $V_{\text{air}} = 12.5$ m/s case (square symbols), the peak frequencies are almost flat about 310Hz until $\phi = 0.65$. Then, strong oscillations are initiated at $\phi = 0.66$ and the peak frequency begins to shift toward higher frequency with the increment of ϕ until it reaches to 0.71. At $\phi = 0.72$ the oscillation amplitude gets small. Beyond this point, two types of trends appear in the plot. One is that the peak frequency increases monotonically against ϕ along the
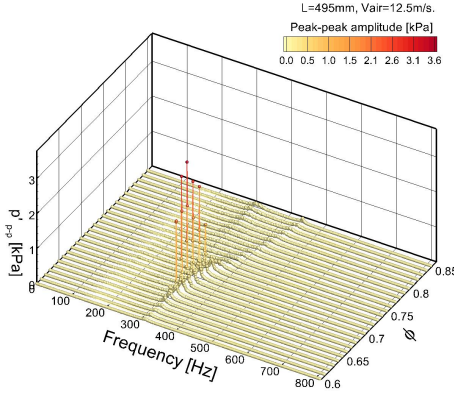
Figure 4: Transition of the pressure power spectrum when increasing equivalence ratio. V_{air}=12.5m/s. Homogeneous mixture case.
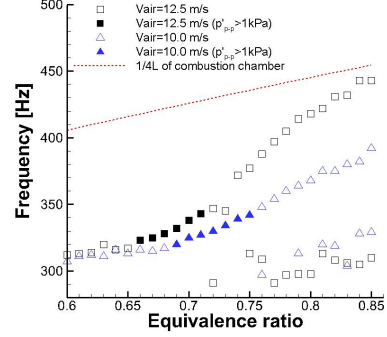

Figure 5: Peak frequencies plot against equivalence ratio. V_{air} = 10.0 and 12.5 m/s. Homogeneous mixture case. Only for the cases of p'_{p-p} > 0.035 kPa are plotted. Filled symbols are the strong oscillation cases (p'_{p-p} > 1.0 kPa).

extension of the frequency shift observed in the strong oscillations range (ϕ = 0.66 – 0.71). The slope of the trend is getting mild for higher equivalence ratios and approaching to the estimated curve of a quarter wave mode of the combustion chamber (indicated by a dashed line). The other is that the frequencies scatter in a narrow band (290–320 Hz) with no clear dependency on ϕ. The overall trend in the case of V_{air} = 10 m/s (triangle symbols) is similar to that of the 12.5 m/s case. Strong oscillations are excited at ϕ = 0.69 and continue until ϕ = 0.76. The range of strong oscillations shifts toward higher equivalence ratios compared to the V_{air} = 12.5 m/s case. Accordingly, the monotonic increase of the low-amplitude peak frequency shift in the same direction. It is noteworthy that the frequency ranges of the strong oscillations in both V_{air} = 10 and 12.5 m/s cases are between 320 and 343 Hz and coincide well each other.

From the observations above, it is indicated that there are at least two types of unstable modes. One is considered the bulk acoustic mode of the system which is composed of the combustion chamber and plenum. The 310 Hz peaks in the lower ϕ range and possibly the peaks in the frequency band between 290 and 320 Hz in the higher ϕ range will be the bulk mode since the peak frequencies are consistent among different velocity and equivalence ratio conditions. Therkelsen et al. [9] applied the general instability model analysis and reported that the measured unstable frequency about 320 Hz corresponded to the first longitudinal mode of the system. It is interesting that the frequency is very close to the unstable frequencies in the present study even though the dimensions of the combustor system are different (for instance, the combustion chamber length was 320mm in their case). Such an acoustic mode analysis is required in our case as well to conclude this point. The other mode seems to be related to the residence time of the shedding vortex from the injector exit to the flame. Increasing the inlet velocity results in the increase of the peak frequencies as can be seen in the difference between the two plots in Figure 5. This suggests that the vortex shedding frequency is increased by the increment of the inlet velocity. Change in the equivalence ratio also modifies the frequency characteristics through the change in speed of sound in the combustion chamber, total mixture flow rate and flame structure. These all effects are believed to be coupled and contributing to the shifting trend in this mode. The strong pressure oscillations are excited when the frequencies of the vortex shedding mode overlapped the bulk acoustic mode. This happened in the frequency range from 320 to 343 Hz as shown in Figure 5.

The translation error (E_{trans}) and damping factor are calculated from the dynamic pressure data for each equivalence ratio and shown in Figure 6. The amplitudes of the first peaks in the power spectra are shown as well for reference. It is obvious that E_{trans} has very low values for ϕ = 0.66–0.71. The minimum E_{trans} is about 0.0017 at ϕ = 0.68. The low E_{trans} range coincides with the range of strong oscillations. As
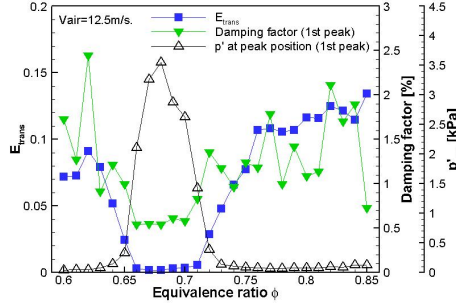
Figure 6: Translation errors (E_{trans}), damping factors and peak amplitudes of the pressure fluctuations. Homogeneous mixture case. V_{air}=12.5m/s.

discussed in the previous study [19], the deterministic chaos produced by the Lorenz equation is treated as low-dimensional chaos, and its E_{trans} is about 0.01. Although the Lorenz equation is not representing the combustion instability, it is useful as an indicator for discussing the degree of complexity of dynamic signals upon the trajectories. The values of E_{trans} in the strong oscillations range (ϕ = 0.66–0.71) are less than 0.01, and therefore, indicate that the data have the deterministic nature in the parallelism of neighboring trajectories. E_{trans} increases in the outside of the strong oscillations range and reaches 0.07 at ϕ = 0.60 and 0.13 at ϕ = 0.85. These values are higher than the criterion and indicate the trajectories of the data are more complicated than that of the low-dimensional chaos. In these ranges, the relative levels of randomness (e.g., due to combustion noise) in the signals are higher than those in the strong oscillations range. This results in the increment of E_{trans}. The damping factors in the strong oscillations range (ϕ = 0.66–0.71) show lower values than those in the outside. However, the overall trend is less clear compared to the E_{trans} plot, especially in the range of weak oscillations. This is considered to be due to the sensitivity of Gaussian fitting for the data around low-amplitude peaks.

Another aspect of the E_{trans} plot is the utilization for monitoring combustor stability margins. As mentioned above, E_{trans} shows more clear transitions between stable and unstable conditions compared to the damping factor. This suggests that the E_{trans} method will be suitable for monitoring the stability margin. Further investigation, for instance, to determine the response time of the calculation, is needed to clarify the capability in this aspect.

4.1.2 Inhomogeneous mixture flame results

Figure 7 shows the pressure power spectra for different fuel split conditions with a constant total equivalence ratio (ϕ_{total} = 0.69). The bulk air velocity is 12.5 m/s. As shown in Figures 4 and 5, ϕ = 0.69 is in the middle of the strong oscillations range of the homogeneous mixture case. The total equivalence ratio 0.69 was chosen as the representative condition to look at the effect of mixture inhomogeneity on the combustion stability. Here, we define λ as the percentage of the downstream fuel flow rate against the total fuel flow rate. It can be seen in Figure 7 that the peak amplitude is very sensitive to the value of λ, while the unstable frequencies stay about 330Hz. This trend is clearly seen in the peak amplitudes plot in Figure 8 (Triangle symbols). In the series of the variable λ experiment, the peak amplitude about 2kPa was observed in the λ = 0 % case (i.e. homogeneous mixture). On the other hand, the peak amplitude is very small (less than 0.2kPa) in the λ = 100 % case (i.e. downstream fuel injection only). There was no linear trend between these conditions. The strongest pressure oscillations are observed around λ = 70–75 %. The peak amplitudes are about 3kPa or more in these conditions. There is also a range of λ (25–40 %) that shows relatively weak oscillation amplitudes. The sensitivity of the oscillation amplitude to λ suggests that there are favorable zones for fuel distribution to enhance (or suppress) combustion instability. Tachibana et al. [26] carried out the traversing LIPS measurement and reported the profiles of the local equivalence ratio along a horizontal line at 10 mm downstream from the inlet of the combustion chamber (fresh gas region). The results are shown in the later section (Figures 10–12). It is important to note that the peak amplitude values have some variations depending on the measure-
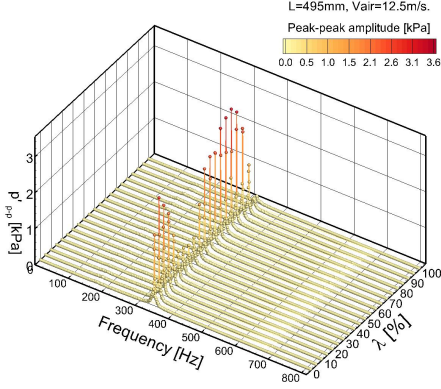
Figure 7: Pressure power spectra for different fuel split conditions (λ=0–100%). Inhomogeneous mixture case. $\phi_{\text{total}} = 0.69$, V_{air}=12.5m/s.
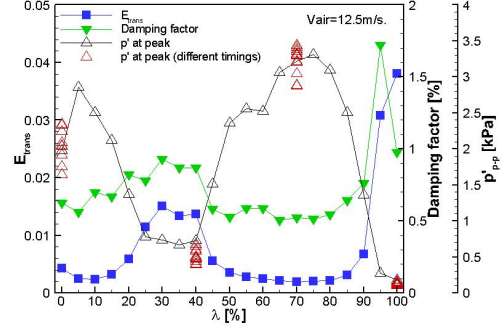

Figure 8: E_{trans}, damping factors and peak amplitudes of the pressure fluctuations against λ. Inhomogeneous mixture case. ϕ_{total}=0.69, V_{air}=12.5m/s.
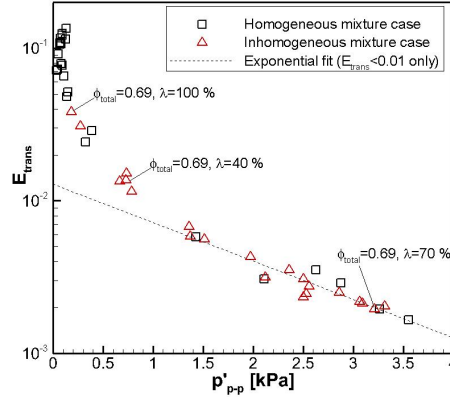

Figure 9: E_{trans} versus peak amplitude. Both homogeneous and inhomogeneous mixture cases (i.e. data in Figures 4 and 7) are shown. Homogeneous case: ϕ = 0.60–0.85, V_{air}=12.5m/s. Inhomogeneous case: ϕ_{total} = 0.69, λ = 0–100 %, V_{air}=12.5m/s.

ment date and time even with the same operation settings. To show these variations, the multiple data taken at different timings are additionally shown in Figure 8 for four λ conditions (λ = 0, 40, 70 and 100 %).

The E_{trans} values in Figure 8 (Square symbols) show transitions corresponding to the pressure oscillation amplitudes. Also, it is obvious that the trend of E_{trans} is more clear than that of the damping factor. Both these features are the same as in the case of homogeneous mixture combustion (See Figure 6).

Figure 9 shows the E_{trans} versus peak amplitude plot. Both homogeneous and inhomogeneous mixture cases (i.e. data in Figures 4 and 7) are shown in the plot. It is interesting to note that the E_{trans} shows an exponential decay with increasing the peak amplitude in the range $E_{\text{trans}} < 0.01$. This is considered another evidence that the dynamic data in the range has a deterministic nature as the same level seen in the low-dimensional chaos. For reference, the E_{trans} calculation of a sinusoidal function data with a single frequency of 330Hz gives the value in the order of 10^{-5}. (Two orders of magnitude less than the present data.)

4.2 Dynamic behaviors of the inhomogeneous mixture flames

The mean OH* intensity and the mean progress variable based on the laser Mie scattering images ($\bar{c}_{Mie}$) of the oil mist are shown in Figures 10–12 for λ = 70, 40, and 100% cases, respectively. The E_{trans} values for these conditions are indicated in Figure 9. Because the flame structures are axisymmetric [26], only the right-hand-side plane distributions are shown (The mean OH* contour maps are flipped to the left hand side). One can immediately find from the OH* intensity distributions that there is no bowl-shaped flame base in the cases of λ = 70 and 40 % (Figures 10 and 11). In contrast, the bowl-shaped flame base is the essential part of the flame stabilization in the λ = 100 % case (Figure 12). The local equivalence ratios at the inlet in the central zones of the λ = 70 and 40 % cases are very low. For instance, ϕ is less than 0.46 (below the lean flammable limit) in -5mm $\leq x \leq$ 5mm at y =10mm. The ultra-lean fresh gas mixture will be mixed with the burnt gas downstream and supposed to be consumed through high-temperature chemical reactions, although it is difficult to estimate how the reactions take place and contribute to the instability mechanism.

Below, we mainly discuss about the dynamic behaviors of the flame structures in a strong and weak oscillation cases, i.e., λ = 70 and 40 %, respectively. Peak pressure amplitude of λ=70% is more than four times larger than that of λ=40% (See Figure 8). In the strong oscillations case (λ = 70%), a cyclic motion of a bulge structure is observed as shown in the $\bar{c}_{Mie}$ contour maps in Figure 10. The bulge appears at the injector rim about $\theta \sim$ 180 deg, moves downstream along the outer shear layer, and finally enters into the large heat-release fluctuating zone near the wall ($\theta \sim$ 120 deg). The velocity field of the unstable CH_4-air homogeneous mixture flame of Therkelesen et al. [9] showed that a ring vortex shed from the rim traveled in the OSL and merged with the stationary ring vortex near the wall. The unsteady behavior of the bulge along the OSL is considered to have a direct relationship with the traveling vortex, even though the flame base stabilization mechanisms are different. Tachibana et al. [26] showed that the phase-resolved profile of the overall integrated OH* intensity had a similar shape with the profile of the pressure oscillations. The phase difference between the OH* and pressure oscillations was small and satisfied the Rayleigh criterion. The maximum and minimum OH* intensities were observed at 60 and 270 degrees, respectively. Figure 10 clearly shows significant heat release variations in the stationary vortex flame region near the wall. The strongest and weakest intensities in the region are seen at θ = 60 and 240 degrees, respectively. This coincides with the trend of the total OH* variations. The bulge of fresh gas, which is considered a traveling vortex ring of fresh gas mixture, is periodically moving along the OSL and merging with the stationary vortex flame near the wall. This periodic motion corresponds well with the dynamic heat-release oscillations.

In the weak oscillations case of λ = 40% (Figure 11), both OH* and $\bar{c}_{Mie}$ variations in one cycle are small compared to the strong oscillations case. In this case also, θ = 60 and 240 degrees, respectively, were almost corresponding to the maximum and minimum of the total OH* intensity profile [26]. The similar trend can be found in Figure 11 but is less clear. Similarly, the unsteadiness of the $\bar{c}_{Mie}$ distribution is small and it is difficult to find the bulge movement.

Another feature of the two flames is that the flames exhibit two arms-like structures extending toward upstream. The locations of these structures are considered to be overlapping the inner and outer shear layers. When comparing the OH* and $\bar{c}_{Mie}$ distributions in Figures 10 and 11, the shapes of the band around $\bar{c}_{Mie}$ = 0.50 (green color in the contour) correspond with the envelope of the flame in the fresh gas side. Both these flame arms along the ISL and OSL are clearly observed for phase angles from 0 to 120 degrees in Figure 11. On the other hand, in Figure 10, the flame along the ISL is more pronounced than that along the OSL. The larger flame oscillation along the ISL in the λ = 70% case is a distinct difference from the λ = 40% flame. Therefore, this is considered to be a key point in the mechanism of the strong combustion instability. The local equivalence ratio profiles for λ = 70 and 40% cases show the local maximums around $x = \pm$ 20 and $\pm$ 25mm, respectively. Richer mixture is supplied to the inner part of the flow in λ =70% case compared to λ = 40 % case. This supports the observation of the longer flame along the ISL for λ = 70% case. These observations indicate that the strong oscillations occur when richer mixtures locate about the ISL. The traveling vortex carries richer mixture to the stationary vortex flame and enhance the interaction between the two vortices. It can be summarized that the driving force of the instability is the vortex-flame interaction, but the strength of the instability is modified by the local distribution of equivalence ratio.
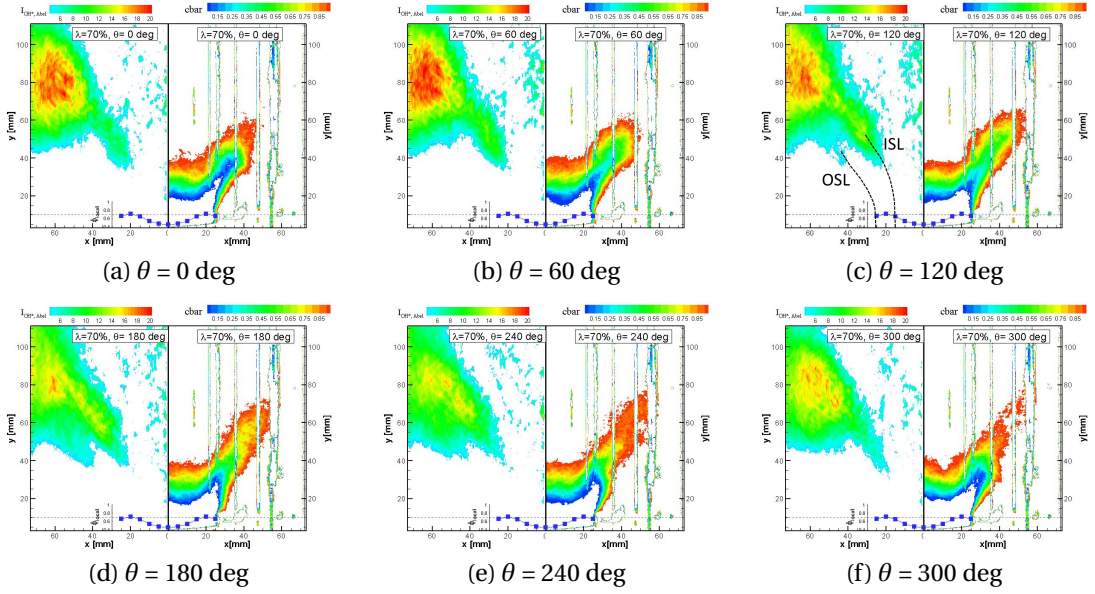
9

(a) $\theta = 0$ deg (b) $\theta = 60$ deg (c) $\theta = 120$ deg

(d) $\theta = 180$ deg (e) $\theta = 240$ deg (f) $\theta = 300$ deg

Figure 10: Phase-resolved mean OH* intensity (left in each figure) and $\bar{c}_{\mathrm{Mie}}$ contour (right in each figure) in the cross-sectional plane. $\lambda = 70\%$, $\phi_{\mathrm{total}} = 0.69$, $V_{\mathrm{air}} = 12.5\,\mathrm{m/s}$. The Abel inversion transform is applied to the mean OH* distributions to show the cross-sectional intensity maps. The actual phase resolution is 30 degrees, but a half of all maps are shown with a skip of 60 degrees in this figure. The plot along the horizontal line at y=10mm is the local mean equivalence ratio profile measured by LIPS [26]. The vertical streaky patterns in the background of the $\bar{c}_{\mathrm{Mie}}$ contours are due to laser sheet reflections on the glass tube surface.

(a) $\theta = 0$ deg (b) $\theta = 60$ deg (c) $\theta = 120$ deg

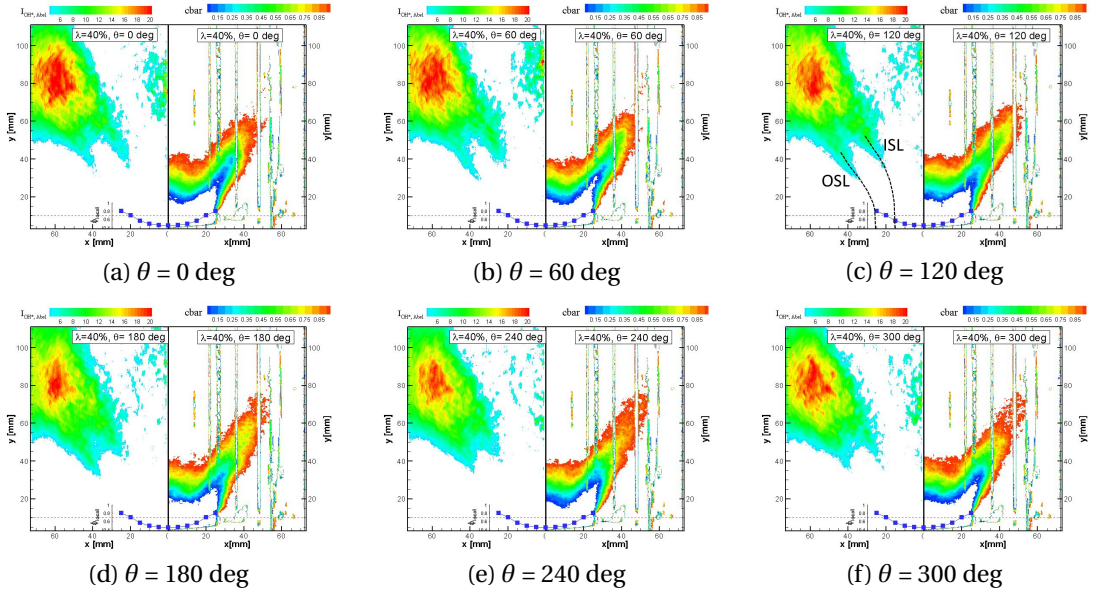(d) $\theta = 180$ deg (e) $\theta = 240$ deg (f) $\theta = 300$ deg

Figure 11: Phase-resolved mean OH* intensity (left in each figure) and $\bar{c}_{\mathrm{Mie}}$ contour (right in each figure) in the cross-sectional plane. $\lambda = 40\%$ case. Other conditions are the same as Figure 10.

(a) θ = 0 deg (b) θ = 60 deg (c) θ = 120 deg

(d) θ = 180 deg (e) θ = 240 deg (f) θ = 300 deg
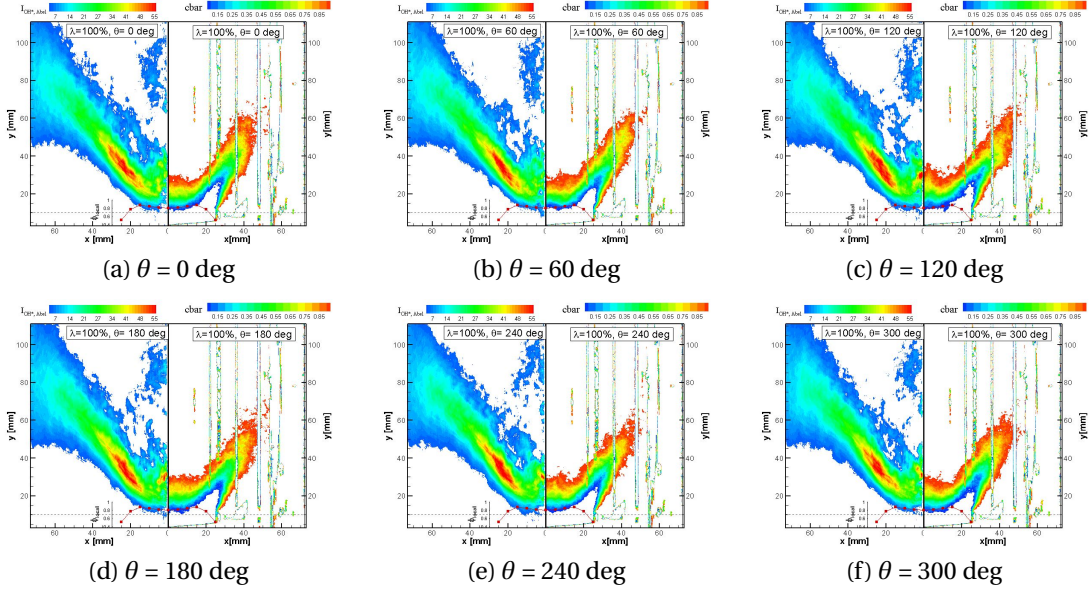
Figure 12: Phase-resolved mean OH* intensity (left in each figure) and $\bar{c}_{\mathrm{Mie}}$ contour (right in each figure) in the cross-sectional plane. λ = 100% case. Other conditions are the same as Figure 10.

In the case of λ =100%, pressure oscillations amplitude was very small (less than 10 % of the λ =70% case). As can be seen in Figure 12, a bowl-shaped flame is stabilized with small intensity variations in phase. No strong intensity is observed in the stationary vortex flame region. This is very contrastive to the observations in Figures 10 and 11. The local equivalence ratios are very rich in the range -20mm $\leq x \leq$ 20mm and rapidly decreases below 0.50 at $x = \pm 25$mm. There is no way to generate strong heat-release fluctuations in the wall impingement region simply because less fuel is supplied in the region.

5 Conclusions

Characteristics of the dynamic pressure data and flame structures in a lean premixed model combustor under self-excited combustion instabilities were investigated. The findings are summarized below.

- The spectral analysis results indicated that there were at least two types of unstable modes in the combustion instability with homogeneous mixture. One was considered the bulk acoustic mode of the system and the other seemed to be related to the residence time of the shedding vortex from the injector exit to flame. The strong pressure oscillations were excited when the frequencies of the two modes overlapped. This happened in the frequency range from 320 to 343 Hz.

- The values of E_{trans} in the strong oscillations range were less than 0.01 (a criterion of the low-dimensional chaos), and therefore, indicated that the data had a deterministic nature in the parallelism of neighboring trajectories. The values of E_{trans} showed an exponential decay with increasing the peak amplitude in the range $E_{\mathrm{trans}} < 0.01$. This will be another evidence that the dynamic data in the range had a deterministic nature.

- E_{trans} showed more clear transitions between stable and unstable conditions compared to the damping factor with the bandwidth method. This suggested that the E_{trans} could be used for monitoring combustor stability margins.

- From the $\bar{c}_{\mathrm{Mie}}$ contour in the strong oscillations case (λ = 70%), a cyclic motion of a bulge structure was observed. The bulge of fresh gas, which was considered a traveling vortex ring of fresh gas

mixture, was periodically moving along the outer shear layer and merging with the stationary vortex flame near the wall. It was difficult to find such a bulge motion in the weak oscillation cases (λ = 40 and 100 %).

- The dynamic flame motions along the ISL and local equivalence ratio distributions in the upstream indicated that the strong oscillations occur when richer mixtures locate about the ISL. In λ =70% case, the traveling vortex was considered to carry richer mixture to the stationary vortex flame and enhanced the interaction between the two vortices. In summary, the driving force of the instability was the vortex-flame interaction, but the strength of the instability was modified by the local distribution of equivalence ratio.

References

[1] T. Lieuwen and V. Yang, editors. *Combustion Instabilities in Gas Turbine Engines: Operational Experience, Fundamental Mechanisms, and Modeling*. AIAA, Reston, VA, 2005.

[2] C.K. Chan, K.S. Lau, W.K. Chin, and R.K. Cheng. Freely propagating open premixed turbulent flames stabilized by swirl. *Proc. Combust. Inst.*, 24(1):511–518, 1992.

[3] R.K. Cheng, D. Littlejohn, W.A. Nazeer, and K.O. Smith. Laboratory studies of the flow field characteristics of low-swirl injectors for application to fuel-flexible turbines. *J. Eng. Gas Turbines Power*, 130(2):21501–21511, 2008.

[4] R.K. Cheng, D. Littlejohn, P. Strakey, and T. Sidwell. Laboratory investigations of low-swirl injectors with H_2 and CH_4 at gas turbine conditions. *Proc. Combust. Inst.*, 32:3001–3009, 2009.

[5] D. Littlejohn, R.K. Cheng, D.R. Noble, and T. Lieuwen. Laboratory investigations of low-swirl injectors operating with syngases. *J. Eng. Gas Turbines Power*, 132(1):011502–011510, 2010.

[6] S. Tachibana, J. Yamashita, L. Zimmer, K. Suzuki, and A.K. Hayashi. Dynamic behavior of a freely-propagating turbulent premixed flame under global stretch-rate oscillations. *Proc. Combust. Inst.*, 32(2):1795–1802, 2009.

[7] D.M. Kang, F.E.C. Culick, and A. Ratner. Combustion dynamics of a low-swirl combustor. *Combust. Flame*, 151(3):412–425, 2007.

[8] Y. Huang and A. Ratner. Experimental investigation of thermoacoustic coupling for low-swirl lean premixed flames. *J. Propul. Power*, 25(2):365–373, 2009.

[9] P. L. Therkelsen, J. E. Portillo, D. Littlejohn, S.M. Martin, and R.K. Cheng. Self-induced unstable behaviors of CH_4 and H_2 /CH_4 flames in a model combustor with a low-swirl injector. *Combust. Flame*, 160:307–321, 2012.

[10] D.W. Davis, P.L. Therkelsen, D. Littlejohn, and R.K. Cheng. Effects of hydrogen on the thermo-acoustics coupling mechanisms of low-swirl injector flames in a model gas turbine combustor. *Proc. Combust. Inst.*, 34(2):3135–3143, 2013.

[11] H. Kantz and T. Schreiber. *Nonlinear Time Series Analysis*. Cambridge University Press, Cambridge, 1997.

[12] C. S. Daw, J. F. Thomas, G. A. Richards, and L. L. Narayanaswami. Chaos in thermal pulse combustion. *Chaos*, 5:662–670, 1995.

[13] A. K. Sen, G. Litak, T. Kaminski, and M. Wendeker. Multifractal and statistical analyses of heat release fluctuations in a spark ignition engine. *Chaos*, 18:033115, 2008.

[14] H. Gotoda, T. Miyano, and I. G. Shepherd. Dynamic properties of unstable motion of swirling premixed flames generated by a change in gravitational orientation. *Phys. Rev. E*, 81:026211, 2010.

[15] L. Kabiraj, A. Saurabh, P. Wahi, and R. I. Sujith. Route to chaos for combustion instability in ducted laminar premixed flames. *Chaos*, 22:023129, 2012.

[16] Andrew C. Noble, Galen B. King, Normand M. Laurendeau, James R. Gord, and Sukesh Roy. Non-lienar thermoacoustic instability dynamics in a rijke tube. *Combustion Science and Technology*, 184(3):293–322, 2012.

[17] Larry K. B. Li and Matthew P. Juniper. Lock-in and quasiperiodicity in hydrodynamically self-excited flames: Experiments and modelling. *Proc. Combust. Inst*, 34:947–954, 2013.

[18] R. Wayland, D. Bromley, D. Pickett, and A. Passamante. Recognizing determinism in a time series. *Phys. Rev. Lett*, 70:580–582, 1993.

[19] H. Gotoda, H. Nikimoto, T. Miyano, and S. Tachibana. Dynamic properties of combustion instability in a lean premixed gas-turbine combustor. *Chaos*, 20:013124, 2011.

[20] H. Gotoda, M. Amano, T. Miyano, T. Ikawa, K. Maki, and S. Tachibana. Characterization of complexities in combustion instability in a lean premixed gas-turbine model combustor. *Chaos*, 22:043128, 2012.

[21] P. Petersson, J. Olofsson, C. Brackman, H. Seyfried, J. Zetterberg, M. Richter, M. Aldén, M.A. Linne, R.K. Cheng, A. Nauert, D. Geyer, and A. Dreizler. Simultaneous PIV/OH-PLIF, Rayleigh thermometry/OH-PLIF and stereo PIV measurements in a low-swirl flame. *Appl. Opt.*, 46(19):3928–3936, 2007.

[22] F. Takens. Detecting strange attractors in turbulence. *in: D. A. Rand and L.-S. Young eds., Dynamical Systems and Turbulence, Lecture Notes in Mathematics, vol. 898, Springer-Verlag.*, pages 366–381, 1981.

[23] E. Laudien, R. Pongratz, R. Pierro, and D. Preclik. Experimental procedures aiding the design of acoustic cavities. *in: V. Yang and W. E. Anderson eds. Liquid Rocket Engine Combustion Instabilities, AIAA, Washington DC.*, pages 377–399, 1995.

[24] T. Lieuwen. Online combustor stability margin assessment using dynamic pressure data. *J. Eng. Gas Turbines Power*, 127:478–482, 2005.

[25] P. Perona and J. Malik. Scale-space and edge detection using anisotropic diffusion. *IEEE Transactions on Pattern Analysis and Machine Intelligence*, 12(7):629–639, 1990.

[26] S. Tachibana, A. Fukumoto, K. Kanai, S. Yoshida, K. Suzuki, and T. Sato. Combustion instability in a lean premixed low-swirl combustor with mixture inhomogeneity. *To be presented at ECM2013, Lund, Sweden*, 2013.